International Soil and Water Conservation Research xxx (xxxx) xxx

Contents lists available at ScienceDirect

International Soil and Water Conservation Research

journal homepage: www.elsevier.com/locate/iswcr

Original Research Article

Distribution patterns of SOC fractions and mineralization on sloping erosion-prone farmland in the black soil region

Mengni Li [a], Qingwen Zhang [a,*], Jeroen Meersmans [b], Aurore Degré [b]

[a] Agricultural Clean Watershed Research Group, Institute of Environment and Sustainable Development in Agriculture, Chinese Academy of Agricultural, Sciences/Key Laboratory of Agricultural and Rural Eco-Environment, Ministry of Agriculture and Rural Affairs, Beijing, 100081, China
[b] Gembloux Agro-BioTech, Biosystem Engineering, Soil–Water–Plant Exchanges, University of Liege, Passage des Déportés, Gembloux, Belgium

ARTICLE INFO

Article history:
Received 2 January 2025
Received in revised form
31 July 2025
Accepted 1 August 2025
Available online xxx

Keywords:
Long gentle sloping farmland
Soil erosion
Soil organic carbon
^{137}Cs
Wavelet analysis

ABSTRACT

Soil organic carbon (SOC), primarily accumulated in the surface layers of sloping farmland, experiences disrupted distribution due to soil erosion, affecting its lateral transport and vertical sequestration. To gain a deeper understanding of the interaction between soil erosion and the carbon cycle, this study assessed the effects of two tillage practices, as slope-ridge tillage (SRT) and cross-ridge tillage (CRT), in controlling soil erosion on long gentle sloping farmland in the Northeast black soil region in China, while evaluating spatial variations in erosion rates, SOC content, and SOC fractions using the Caesium-137 (^{137}Cs) technique combined with wavelet analysis. The findings revealed lower ^{137}Cs inventories for both SRT (732.96 Bq·m^{-2}) and CRT (1000.98 Bq·m^{-2}) compared to the reference value (2468.77 Bq·m^{-2}), confirming the occurrence of soil erosion. CRT showed a significantly lower erosion rate (3056.65 t km^2·a^{-1}) than SRT (4409.04 t km^2·a^{-1}), indicating greater effectiveness in erosion control. Wavelet analysis further uncovered periodic erosion-deposition patterns under both tillage practices, which corresponded to variations in SOC content and its fractions. A significant negative correlation was observed between SOC content and cumulative mineralization, with soil erosion rate emerging as a critical driver of these relationships. Correlation analysis confirmed that SOC fractions play a crucial role in driving SOC mineralization and are intricately linked with SOC dynamics. Random forest analysis identified soil erosion rate, SOC, and dissolved organic carbon (DOC) content as key factors influencing SOC mineralization under SRT. The findings suggest that CRT is more effective in reducing soil erosion by modifying microtopography, thereby minimizing the migration of mineral-associated organic carbon (MAOC) and enhancing SOC retention. This research provides critical insights for developing sustainable land management practices in the region, mitigating the adverse impacts of erosion on the carbon cycle.

1. Introduction

Soil erosion, a significant physical-geographical process poses a severe threat to terrestrial ecosystems by driving global soil degradation. It is widely recognized as a key driver of soil organic carbon (SOC) migration, loss, and redistribution, exerting profound impacts on the terrestrial carbon (C) cycle (Borrelli et al., 2017; Lal, 2005, 2019; Mariappan et al., 2022). During soil erosion processes, runoff interacting with soil particles generates fine particles that transport SOC downslope. These particles eventually become buried in deposition areas, reorganizing SOC distribution patterns (Ganasri & Ramesh, 2016; He et al., 2023; Saha et al., 2018). As soil erosion redistributes SOC across different landscape positions, low-lying areas tend to accumulate deposited SOC, while soluble substances can be leached and transported to surface waters and the atmosphere, accelerating SOC mineralization (Liu et al., 2023; Wei et al., 2014). This redistribution affects SOC content and intensifies carbon exchange between the soil and atmosphere, potentially accelerating SOC mineralization (Lal, 2003; Van Hemelryck et al., 2011; Xiao et al.,

* Corresponding author.
E-mail address: zhangqingwen@caas.cn (Q. Zhang).

Peer review under the responsibility of International Research and Training Center on Erosion and Sedimentation, the China Water and Power Press, and China Institute of Water Resources and Hydropower Research.

https://doi.org/10.1016/j.iswcr.2025.08.001

2018). Even minor changes in SOC mineralization can significantly influence atmospheric carbon dioxide (CO_2), highlighting the critical role of SOC dynamics in regulating global climate change (Lal et al., 2015). Sloping farmland, particularly susceptible to SOC loss via runoff and sediment transport underscores the need to understand lateral SOC migration and loss patterns for developing effective erosion mitigation strategies.

Despite significant differences in the redistribution of SOC along slopes, there remains a critical gap in scientific data to quantitatively assess how water erosion influences SOC fraction distribution and subsequent C emissions (Wang et al., 2013; Zhou et al., 2024). Previous studies have shown that eroded areas primarily accumulate active organic carbon, which inadequately offsets overall SOC losses (Lal & Pimentel, 2008; Van Oost et al., 2007). The recovery of more stable SOC fractions, such as mineral-associated organic carbon (MAOC), is significantly slower, resulting in sustained SOC declines. Key indicators of SOC variability, including dissolved organic carbon (DOC) and particulate organic carbon (POC), are particularly sensitive to soil erosion processes (Dong et al., 2022; Fultz et al., 2013). When soil aggregates break due to erosion and lose their physical protection, the exposed soil organic matter (SOM) decomposes more easily through microbial activity, accelerating CO_2 emissions into the atmosphere (Dungait et al., 2013). Recalcitrant organic carbon (ROC), which cycles rapidly, serves as an important indicator of SOM quality and is highly responsive to environmental changes (Zhao et al., 2018). The selective migration of SOC fractions during erosion alters SOC structure, with varying C fractions exhibiting distinct responses to environmental shifts (von Lützow et al., 2008).

Therefore, these processes highlight the critical role of the erosion-induced SOC fractions migration in both SOC stabilization and C emissions. Considering that sloping farmland is a primary source of soil erosion, largely driven by the combined effects of raindrop impact and runoff, gaining insights into the lateral migration and loss patterns of SOC and its fractions along slopes becomes imperative. The hypothesis is that SOC fractions are crucial in driving SOC mineralization on erosion prone sloping farmland and are intricately linked to SOC dynamics. Understanding the erosion-induced migration of SOC fractions is crucial for assessing the broader implications of soil erosion on C dynamics and climate change.

The Black soil region of Northeast China, a vital grain production region, faces intensified soil erosion and SOM loss due to the transition from natural to intensive farming systems, leading to significant C emissions (Wang et al., 2020). Unsustainable agricultural practices exacerbate soil erosion, accelerating soil degradation, reducing farmland productivity, and threatening food security and ecological sustainability (Shu et al., 2023). In this region, sloping farmland subjected to different tillage practices, such as contour ridge tillage (CRT) and traditional longitudinal-ridge tillage, experiences varying erosion intensities and SOC redistribution patterns (Guo et al., 2019; Xu et al., 2018). As a form of contour farming, CRT mitigates soil erosion and deposition on long gentle sloping farmland, improves erosion control, and promotes the equalization of SOC and nutrients distribution, ultimately reshaping the spatial distribution of SOC (Li et al., 2024).

The fallout radioactive isotope Caesium-137 (^{137}Cs), an effective tracer for estimating soil redistribution, has been used to reveal periodic fluctuations in erosion intensity across slopes (Li et al., 2006, 2007; Zhang & Li, 2014). Following its deposition, ^{137}Cs is rapidly adsorbed by fine soil particles and SOM, migrating along with eroded soil, making it an effective tracer for estimating soil redistribution. Previous studies have documented spatial variations in soil erosion intensity and SOC redistribution along slopes (Cui et al., 2007; Koomson et al., 2020; Li et al., 2024; Liu et al., 2006). Shen utilized ^{137}Cs to demonstrate periodic erosion intensity fluctuations across the sloping farmland of the Northeast Black Soil Region (Shen et al., 2023). Understanding the periodic variation patterns of soil erosion and deposition rates on hillslopes is crucial for assessing soil degradation and implementing effective soil management strategies.

Wavelet analysis, a powerful mathematical and signal-processing tool (Aliakbardoust et al., 2024; Nason & Sapatinas, 2002; Zhang et al., 2024; Zhu et al., 2024), enables signal reconstruction via wavelet representation and facilitates multi-scale decomposition of series data. This technique interprets the periodic variation characteristics of the original signal across different scales, facilitating frequency-domain analysis. By leveraging the multi-resolution capabilities of wavelet transform operations, this study aims to gain deeper insights into the periodic patterns of slope soil erosion and deposition rates, which impact the SOC fraction distribution and subsequent C emissions.

To bridge existing knowledge gaps and enhance the understanding of SOC redistribution in eroded black soil farmland landscapes, the objective of this study was to investigate the dynamic redistribution traits of SOC and its constituent components. More specifically, this research focused on: (1) exploring the spatial variability of soil erosion-deposition rates along sloping farmland under two distinct tillage practices, combined using ^{137}Cs tracing and wavelet analysis; (2) assessing the spatial disparities in SOC fractions and SOC mineralization rates along the slope; and (3) unveiling the connections between erosion-deposition rates and redistribution patterns of SOC and its fractions.

2. Materials and methods

2.1. The study area

This study site was selected in a typical long gentle sloping farmland of Hongxing Farm (48°02′N-48°17′N, 126°47′E−127°15′E), located in Bei'an City, Heilongjiang Province, a region with nearly 75 years of reclamation history, where ridge construction is performed annually in autumn. The soil in this region is predominantly Mollisols, and the climate is categorized as Monsoon-influenced warm-summer humid continental type. The region experiences an annual average temperature of 2.4 °C, and an average annual precipitation of 555.3 mm. Rainfall is concentrated from July to September, featuring short duration and high-intensity rainstorms. The terrain gently slopes from east to west, with rolling hilltops. Slopes in the study area span from 500 to 1000 m in length, with gradients ranging between 3° and 8°. Notably, the sloping farmland is prone to substantial soil and water loss, with the main tillage practices being traditional slope-ridge tillage (SRT) and cross-ridge tillage (CRT), primarily with crop rotations of corn and soybeans (Fig. 1).

2.2. Sample collection and processing

Sampling was conducted after the entire rainy season and prior to crop harvest in September 2022, when limited human disturbance to the soil was ensured. The ^{137}Cs reference value for the study area was determined by selecting undisturbed grasslands with minimal or no erosion near the study site as the sample plot. The collection point for determination of the ^{137}Cs reference was strategically located near the study area, ensuring an even distribution of ^{137}Cs inventory in the soil profile. Soil samples were collected from a depth of 0–30 cm at 5 cm intervals. A total of thirty samples were collected.

The cultivated land selected for this study was approximately

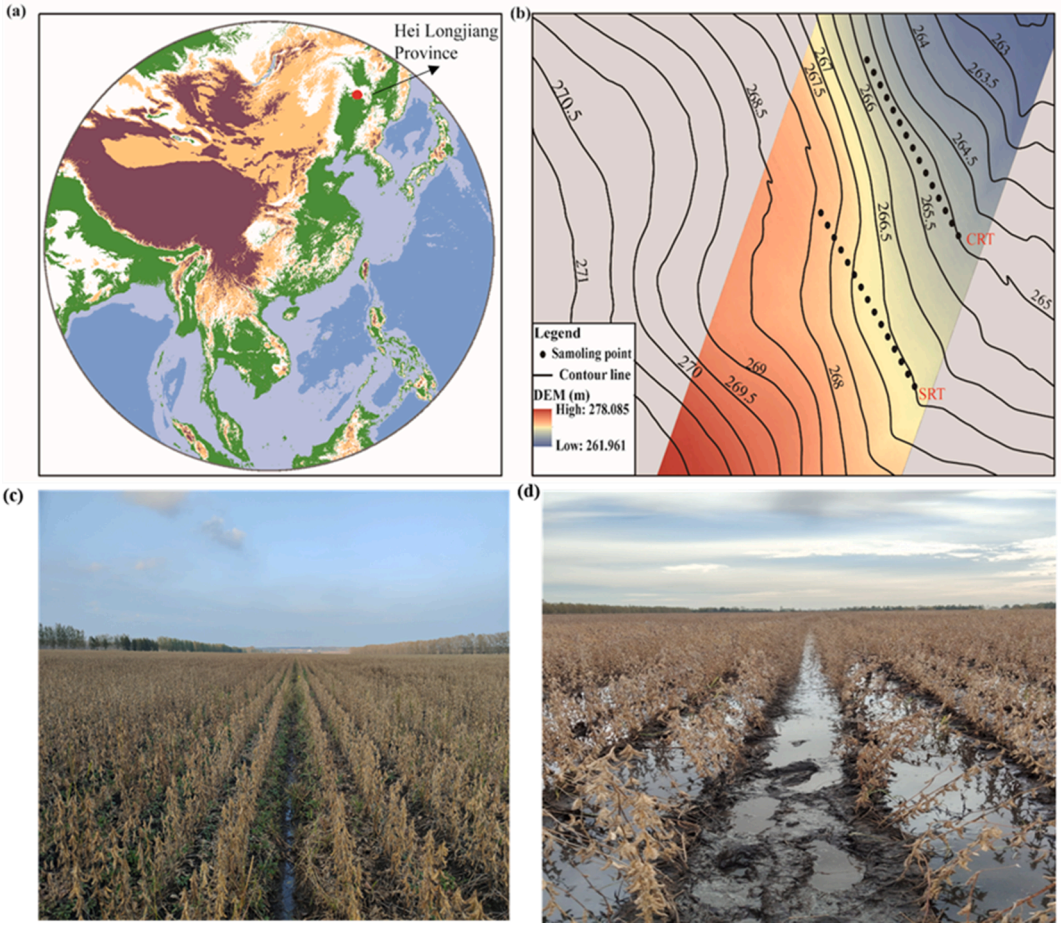

Fig. 1. Study area. (a) Overview of the Heilongjiang province and study area; (b) Spatial distribution of sampling sites (n = 30). (c)(d) Soil sampling locations.

300 m long and 150 m wide. Two types of slopes, SRT and CRT, both of which were straight, were selected for analysis. Sampling was systematically conducted at intervals of 10 m along the longitudinal section of the slope, with a depth of 30 cm for each sample. A total of 15 sampling points were selected on each slope. GPS was used to accurately record the location information of each point. At each sampling point, 5 samples were collected and thoroughly mixed to ensure homogeneity. The soil samples were immediately transported to the laboratory for air drying, grinding, and sieving through 0.25 mm and 2 mm meshes. The soil fraction passing through the 0.25 mm mesh was used for the determination of SOC fractions. Approximately 300 g of soil was weighed at each sampling point and packed for further testing. The measurement of ^{137}Cs was conducted using a high-purity germanium γ spectrometer (Ortec Gmx-50220, Ametek, USA). The ^{137}Cs inventory was calculated based on the full peak area of 661.6 keV γ-rays. Each sample was measured for a duration of 40,000 s, and the instrument's repeatability error was found be to ≤5 % at a 95 % confidence level, ensuring the accuracy and reliability of the results.

Laboratory analyses included determination of soil texture, SOC, and carbon fraction content. Soil texture, namely sand (2–0.05 mm), silt (0.05–0.002 mm) and clay (<0.002 mm) percentages, were determined using the hydrometer method. The SOC components of all samples were meticulously analyzed using an N/C analyzer (multi N/C 2100S, Analytik Jena, Germany). The SOC content was determined through the dry combustion method (Nelson & Sommers, 1996). The DOC was extracted with ultrapure water for 30 min, followed by filtration through 0.45 μm membranes (Jones & Willett, 2006), and subsequently analyzed. The POC was determined following the method outlined by Cambardella and Elliott (1992). Air-dried soil was sieved through a 2 mm mesh to remove visible plant roots and debris. The 10 g of soil sample were then weighed and placed into a plastic bottle. Fifty milliliters of 5 g L^{-1} sodium hexametaphosphate solution were added, and the mixture was dispersed on a reciprocating shaker for 15 h. After dispersion, the soil mixture was placed on a 53 μm sieve and rinsed with distilled water until the leached liquid was clear. The remaining soil sample (>53 μm) was collected into a pre-weighed aluminum box, dried at 60 °C for 48 h, and then weighed. The soil was subsequently ground and passed through a 100 m sieve to determine the total C content. The MAOC (<53 μm) was determined using the difference method.

The ROC content was determined following the method described by Blair et al. (1995). For the analysis, 1.5 g of air-dried soil, sieved through a 0.25 mm mesh, was weighed into a 50 mL centrifuge tube. Then, 25 mL of 333 mmol L^{-1} potassium permanganate was added, and the mixture was shaken for 1 h. Both blank and soil samples were shaken for 1 h. The soil samples were prepared in triplicate to ensure accuracy. After shaking, 1–2 mL of the solution was transferred into a 2 mL centrifuge tube and centrifuged three times at 2000 rpm for 3 min using a high-speed centrifuge. A 100 μL aliquot of the supernatant was pipetted, mixed with 25 mL of deionized water, and diluted 250-fold. The diluted solution was analyzed colorimetrically using a spectrophotometer at a wavelength of 565 nm. The $KMnO_4$ consumption

was calculated based on its concentration change, and the active organic carbon content in the soil was subsequently determined.

2.3. Calculation of ^{137}Cs content per unit area

The ^{137}Cs inventory was first calculated in units of Bq kg^{-1} and then converted to an area inventory (Bq m^{-2}) using the sampling area and bulk density of the soil, following the method described by Zhang et al. (2006):

$$Cs = \sum_{i=1}^{n} C_i \cdot BD_i \cdot DI_i \cdot 10^3 \quad (1)$$

where i represents the sampling layer number; n is the total number of sampling layers; C_i denotes the ^{137}Cs inventory in the i-th sampling layer (Bq·kg^{-1}); BD_i is the soil bulk density of the i-th sampling layer (kg·m^{-3}); and DI_i is the depth of the i-th sampling layer (m).

2.4. Soil erosion calculation model

Soil erosion rate in farmland was estimated using the following formula (Walling et al., 2002; X. Zhang et al., 1990):

$$Cs = A_0 \cdot \left(1 - \frac{\Delta H}{H}\right)^{N-1963} \quad (2)$$

where C_s represents the inventory of ^{137}Cs in the soil profile (Bq·m^{-2}); A_0 denotes the measured reference value of ^{137}Cs, which is 2468.77 Bq·m^{-2}; H indicates the thickness of the tillage layer (m); ΔH is the average annual soil loss thickness (cm·a^{-1}); and N represents the sampling year.

The average annual soil erosion rate was subsequently calculated by integrating the aforementioned average annual soil loss thickness with the soil bulk density using the following formula:

$$E = \rho \cdot h \cdot 10^4 \quad (3)$$

where E represents the annual average soil erosion rate (t·km^{-2}·a^{-1}); ρ denotes the soil bulk density (g·cm^{-3}); h indicates the thickness of the cultivated layer (m); and 10^4 serves as the unit conversion coefficient.

2.5. Wavelet analysis theory

Wavelet analysis is a mathematical tool that reconstructs signals through wavelet representation and facilitates multi-scale decomposition of time series data, thereby elucidating the periodic variation characteristics of the original signal across different scales. Wavelet transform operations enable analysis in both the time and frequency domains and possess characteristics of time-frequency localization and multi-resolution (Nason & Sapatinas, 2002). This study employed wavelet analysis to elucidate the periodic variation patterns of slope soil erosion and deposition rates. Specifically, the continuous wavelet transform is defined by Boros (1999):

$$W(a,b) = \frac{1}{\sqrt{a}} \int f(t) \cdot \varphi^* \cdot \left(\frac{t-b}{a}\right) dt \quad (4)$$

In the formula, $x(t)$ denotes the original signal; $\varphi(t)$ represents the wavelet mother function; a is the scale factor; b is the displacement factor; φ^* indicates the complex conjugate of the wavelet function; and the integral result $W(a,b)$ signifies the wavelet coefficient, reflecting the strength of the correlation between the wavelet function and the original signal at scale a and displacement b.

Among the various wavelet mother functions, the complex Morlet wavelet effectively extracts the strength and phase information of characteristic time scale signals at different times, eliminates false oscillations generated by using the real wavelet transform coefficient as the criterion, and lacks orthogonality. Consequently, the complex Morlet wavelet was selected for the continuous wavelet transform in this study, and its mother wavelet is generally expressed as follows (He et al., 2011):

$$\varphi(t) = \frac{1}{\sqrt{\pi f_b}} \exp\left[-\frac{t^2}{f_b} + 2i\pi f_c t\right] \quad (5)$$

In the formula, f_b denotes the wavelet bandwidth, f_c denotes the wavelet center frequency, and i represents an imaginary number. In this study, the optimal bandwidth f_b was determined to be 1, and the center frequency f_c was also determined to be 1, based on the actual effects of the wavelet transform.

The wavelet stretching scale a is not equivalent to the actual period scale. The stretching scale a and the period T are related as follows:

$$T = \frac{4\pi}{\omega + \sqrt{2+\omega^2}} \cdot a \quad (6)$$

In the formula $\omega = 2\pi f_c$, where f_c represents the center frequency of the wavelet, the actual period scale corresponding to the slope length is:

$$T = 0.520a \quad (7)$$

Wavelet variance reflects the distribution of fluctuation energy across different scales and can objectively and effectively identify the dominant period present in the analyzed sequence. The scale corresponding to the peak of the variance represents the dominant period scale of the sequence. A larger wavelet variance indicates more pronounced periodic characteristics of the signal at the corresponding scale.

$$\mathrm{Var}(a) = \frac{1}{n} \sum_{t=1}^{n} |W(a, x_t)|^2 \quad (8)$$

In the formula, Var denotes the wavelet variance; W represents the wavelet coefficient; $|W|$ indicates the magnitude of the wavelet coefficient; x_t is the time series; and n is the total number of wavelet coefficients obtained at a specific scale. The wavelet variance reflects the distribution of fluctuation energy across scales. The slope length scales a corresponding to each extreme value in the wavelet variance diagram signify the presence of a significant oscillation period within the slope length sequence.

2.6. Statistical analysis

The data obtained from the experiment were organized and analyzed using Microsoft Excel 2016. Due to the limited number of data samples (15 per slope) in this study, MATLAB 2019b was utilized to interpolate and symmetrically expand the data at both ends prior to wavelet analysis. The wavelet variance was computed, and a corresponding wavelet variance map was generated. Origin was employed to create the spatial distribution map of erosion rates. Linear regression analysis was conducted to examine the relationship between erosion and SOC fractions. Additionally, Pearson correlation analysis was performed to quantify the relationships between SOC and C fractions across various tillage practices. The Random Forest (RF) model was utilized to assess the significance of soil erosion and SOC fractions in relation to SOC mineralization and to rank these factors. All

statistical analyses and data visualizations were executed using R v.4.3.0.

3. Results

3.1. Spatial variation of ^{137}Cs content and erosion rate on slopes

The average ^{137}Cs value calculated for the sampling area was 2468.77 Bq·m^{-2}. Consulting existing data confirmed that this reference value falls within the measured range of ^{137}Cs in the black soil region of Northeast China. Thus, the ^{137}Cs reference value of 2468.77 Bq·m^{-2} determined in this study was used to quantitatively assess the soil erosion status of the local watershed.

The area activity of ^{137}Cs at various points on the slope of the sloping farmland ranged from 250.10 to 1488.76 Bq·m^{-2}, all of which were lower than the background value in the study area, indicating that the soil redistribution process was predominantly influenced by soil erosion. In SRT, the minimum and maximum area activities of ^{137}Cs were 250.10 Bq·m^{-2} and 1349.72 Bq·m^{-2}, respectively. For CRT, the minimum and maximum area activities of ^{137}Cs were 615.36 Bq·m^{-2} and 1488.76 Bq·m^{-2}, respectively, with coefficients of variation of 13.03 % and 11.10 %. Compared to the background value, the fluctuation range of the ^{137}Cs area activity on sloping farmland was larger, and the variability in SRT was greater than that in CRT. The redistribution of ^{137}Cs along with soil particles in sloping farmland was significant, and there were notable differences between the various tillage practices. Consequently, soil on the hillslopes has experienced varying degrees of loss.

Based on the results from measurements of the environmental radionuclide ^{137}Cs, the average erosion rate for SRT was greater than that for CRT. The erosion-deposition rates for SRT and CRT ranged from 2024.73 to 7258.97 t km^{-2} a^{-1} and 1696.81 to 4719.68 t km^{-2} a^{-1}, respectively, with average values of 4409.04 t km^{-2} a^{-1} and 3056.65 t km^{-2} a^{-1}. These findings indicate that CRT was more effective at reducing erosion compared to SRT (see Fig. 2).

The spatial distribution of the erosion-deposition rate exhibits pronounced periodic fluctuations (Fig. 3). To further investigate the distribution pattern of the erosion rate under different tillage practices, this study employed wavelet analysis to examine the specific periodic variation of slope erosion rates. Two notable peaks were evident on the SRT hillslope, occurring at slope lengths of 64 m and 88 m (Fig. 4(a)). The corresponding period scales, converted into actual slope lengths using formula (6), were 33.3 m and 45.8 m, respectively. There were two obvious peaks on the CRT slope (Fig. 4(d)), which correspond to the slope length scales of 38 m and 116 m respectively. The period scales converted into actual slope lengths using formula (6) were 19.8 m and 60.3 m, respectively.

3.2. Spatial distribution of soil texture on slopes

Further analysis of soil texture on the slope revealed that the silt content consistently accounted for approximately 50 % of the soil across both tillage practices (Fig. 5), making it the predominant soil fraction. Under SRT, the content of silt (0.002–0.05 mm) and clay (<0.002 mm) initially increased and then decreased along the slope length, whereas the sand (0.05–2 mm) content exhibited an opposite trend. In contrast, under CRT, the contents of silt, clay, and sand displayed periodic variation along the slope length.

3.3. Distribution of carbon fractions and mineralization on slopes

The mean SOC value for the SRT hillslope was 23.51 g kg^{-1}, ranging from 10.11 to 37.54 g kg^{-1} (Fig. 6(a)). The average DOC content was 40.18 mg kg^{-1}, with a range of 32.16–59.40 mg kg^{-1} (Fig. 6(b)). The mean ROC value was 5.30 mg kg^{-1}, varying between 3.30 and 8.44 mg kg^{-1} (Fig. 6(c)). The average POC content was 8.74 g kg^{-1}, ranging from 3.80 to 18.70 g kg^{-1} (Fig. 6(d)). Lastly, the mean MAOC value was 14.82 g kg^{-1}, with a range of 6.32–20.14 g kg^{-1} (Fig. 6(e)).

The mean value of SOC for the CRT hillslope was 27.51 g kg^{-1}, with a range of 19.29–34.26 g kg^{-1} (Fig. 6(a)). The average value of DOC was 32.34 mg kg^{-1}, ranging from 19.29 to 63.25 mg kg^{-1} (Fig. 6(b)). The mean value of ROC was 7.62 mg kg^{-1}, with values ranging from 3.90 to 10.04 mg kg^{-1} (Fig. 6(c)). The average value of POC was 9.54 g kg^{-1}, ranging from 2.81 to 15.36 g kg^{-1} (Fig. 6(d)). Finally, the mean value of MAOC was 18.25 g kg^{-1}, with a range from 13.24 to 28.33 g kg^{-1} (Fig. 6(e)).

The mean SOC cumulative mineralization for the SRT hillslope was 51.15 mg kg^{-1}, with a range of 32.88–85.35 mg kg^{-1} (Fig. 6(f)). In contrast, the mean SOC cumulative mineralization for the CRT hillslope was 65.48 mg kg^{-1}, ranging from 40.50 to 97.64 mg kg^{-1} (Fig. 6(f)).

3.4. Response of SOC fractions to erosion

3.4.1. Relationship between soil erosion and SOC fractions

Regression analysis was performed to investigate the relationship between various C components and the soil erosion rate (Fig. 7). Across different tillage practices, SOC content demonstrated a significant negative correlation with the average annual soil erosion rate ($p < 0.01$, Fig. 7(a) and (b)). Notably, with the exception of MAOC in CRT (Fig. 7(e)), where the negative correlation with the average annual soil erosion rate was not statistically significant ($p > 0.05$), all other SOC fractions showed a significant negative correlation ($p < 0.05$). This indicates that SOC

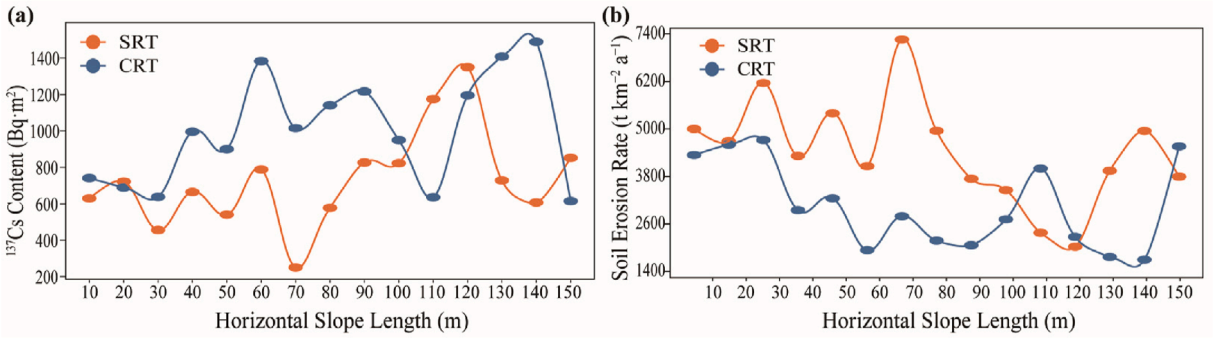

Fig. 2. Variation of ^{137}Cs area activity (a) and average soil erosion rate (b) with slope length on surfaces under SRT and CRT tillage practices.

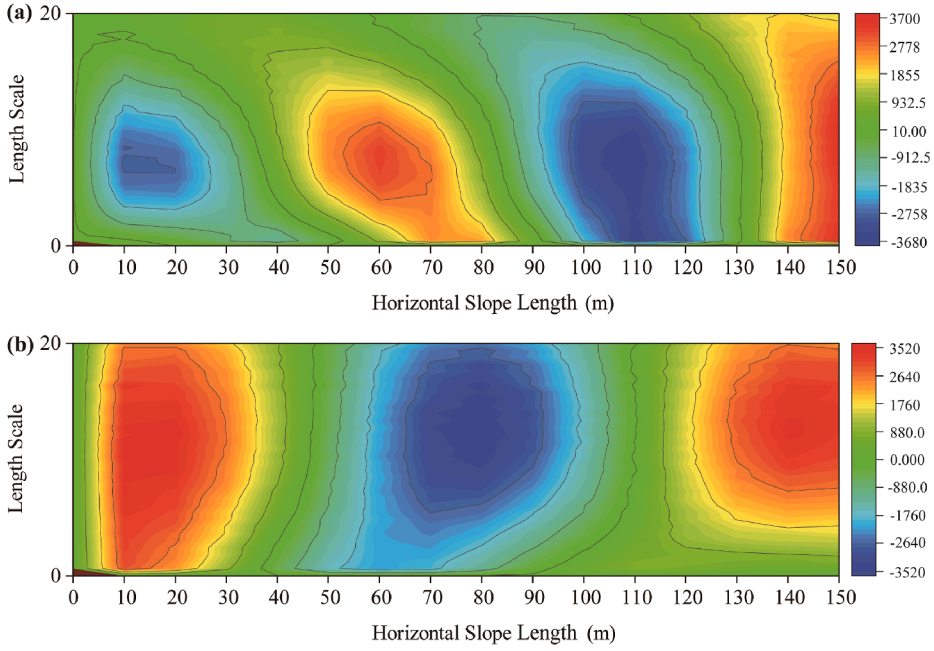

Fig. 3. Spatial distribution of erosion-deposition rates on slope surfaces under SRT(a) and CRT(b).

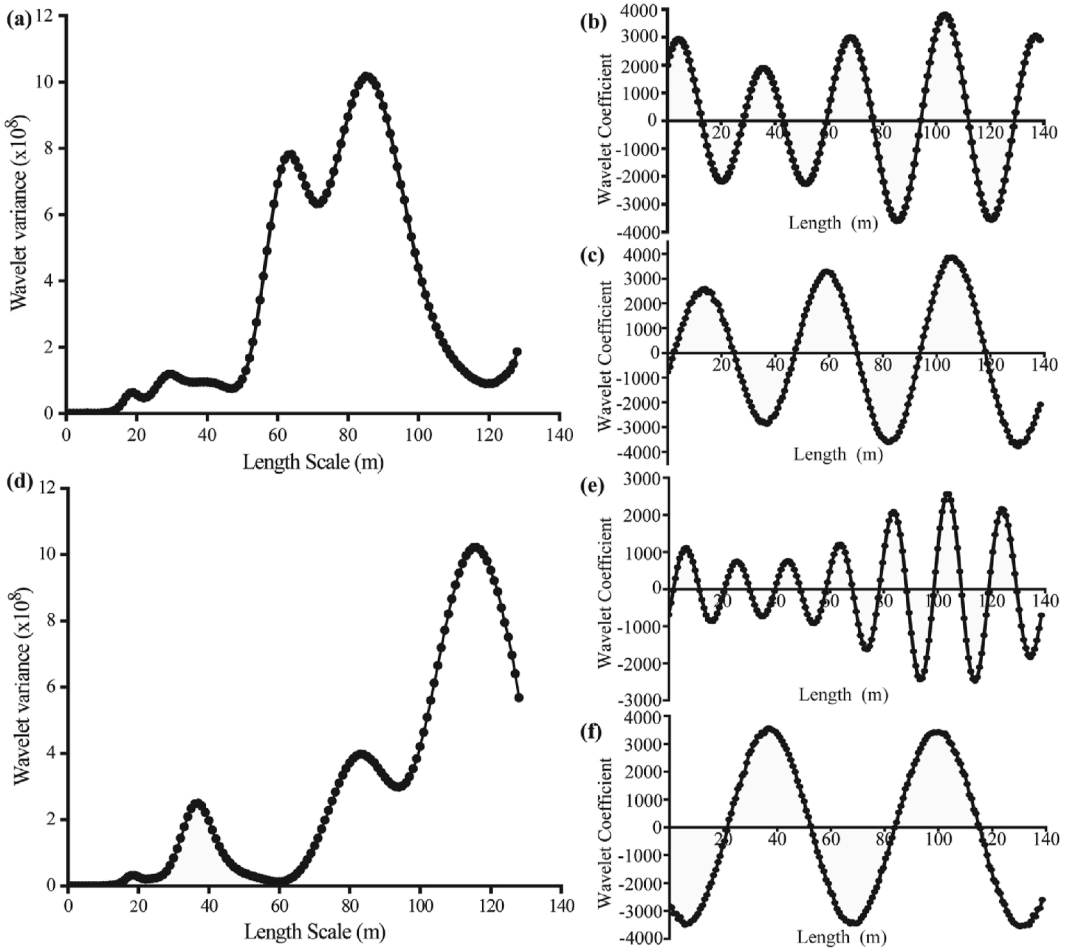

Fig. 4. Wavelet variation of soil erosion rates on slope surfaces under SRT(a) and CRT(d); Wavelet coefficient variation of soil erosion rates at the 64 m slope length scale under SRT (b); Wavelet coefficient variation of soil erosion rates at the 88 m slope length scale under SRT(c); Wavelet coefficient variation of soil erosion rates at the 38 m slope length scale under CRT(e); Wavelet coefficient variation of soil erosion rates at the 116 m slope length scale under CRT(f).

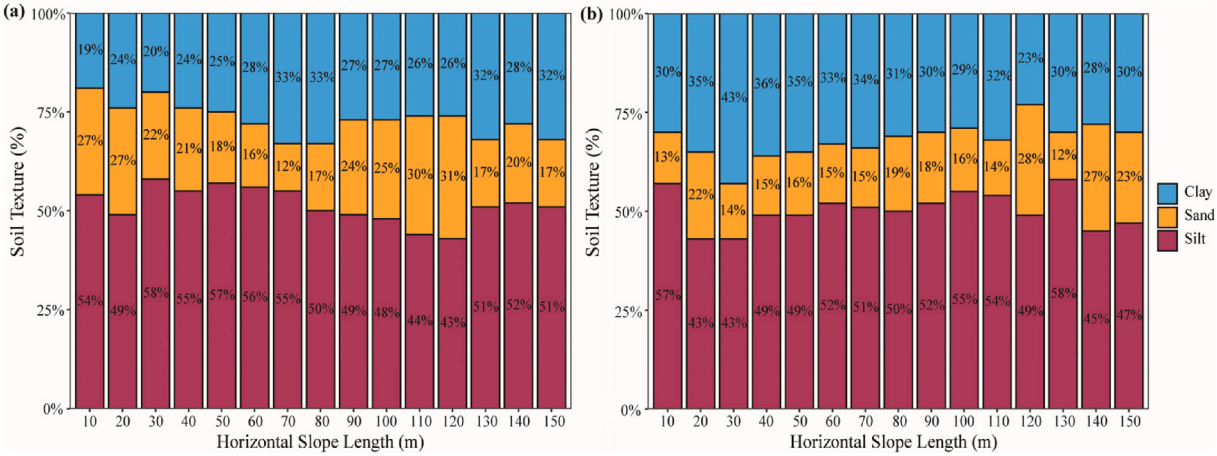

Fig. 5. Variation of soil texture along slope length under (a) SRT and (b) CRT.

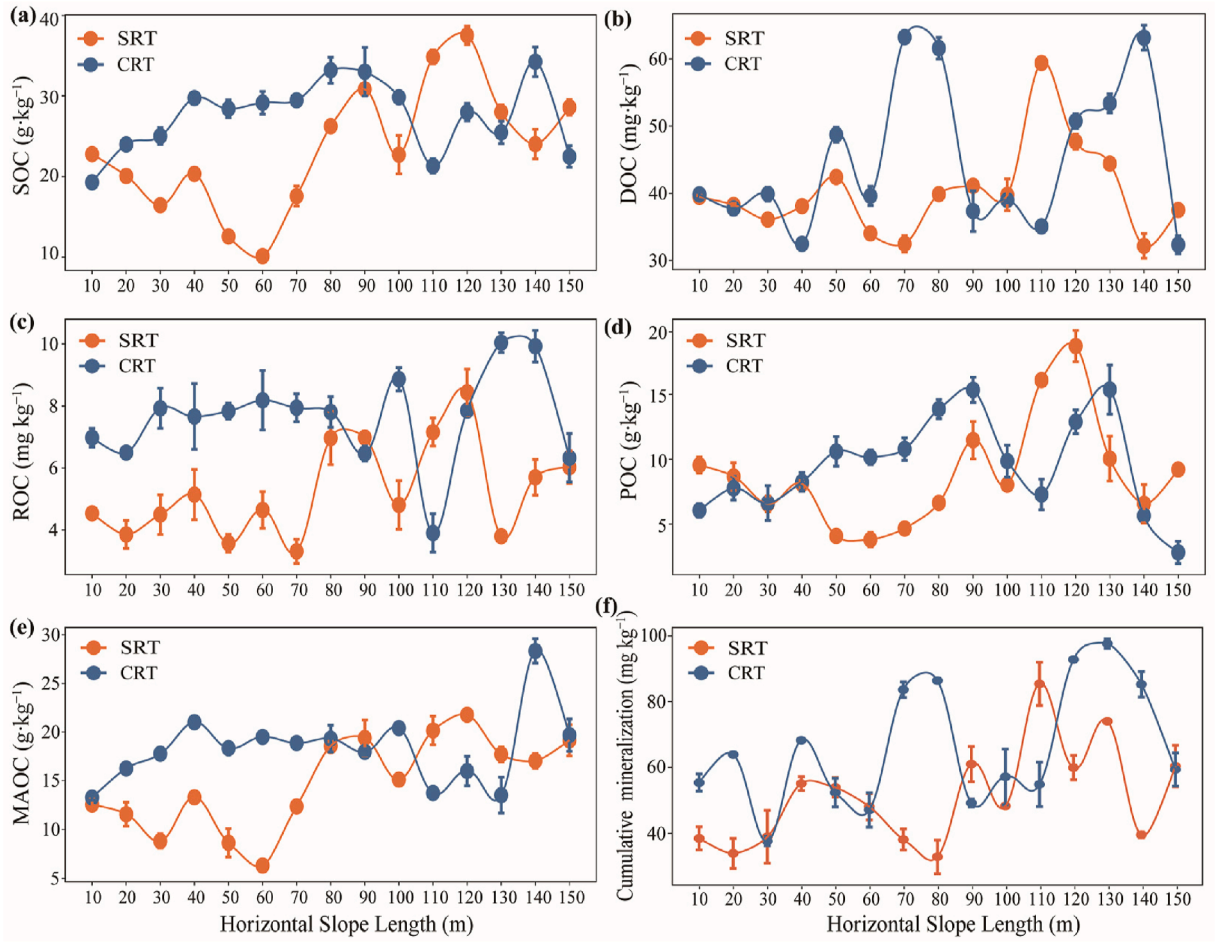

Fig. 6. Variation of SOC fractions and cumulative mineralization along slope length. SOC: Soil organic carbon; DOC: Dissolved organic carbon; ROC: Recalcitrant organic carbon; POC: particulate organic carbon; MAOC: Mineral-associated organic carbon.

content declined markedly as the erosion rate increased. Furthermore, the SOC cumulative mineralization exhibited a significant negative correlation with variations in soil erosion rate along the slope length ($p < 0.05$). These findings emphasize that higher erosion rates are associated with substantial reductions in both SOC content and mineralization, underscoring the critical impact of soil erosion on SOC dynamics in sloping farmland.

Under SRT, sand content exhibited a significant negative correlation with the amount of erosion ($p < 0.01$, Fig. 7(g)), while silt content showed an extremely significant positive correlation ($p < 0.001$, Fig. 7(h)). In contrast, clay content displayed no significant correlation with the amount of erosion ($p > 0.05$, Fig. 7(h)).

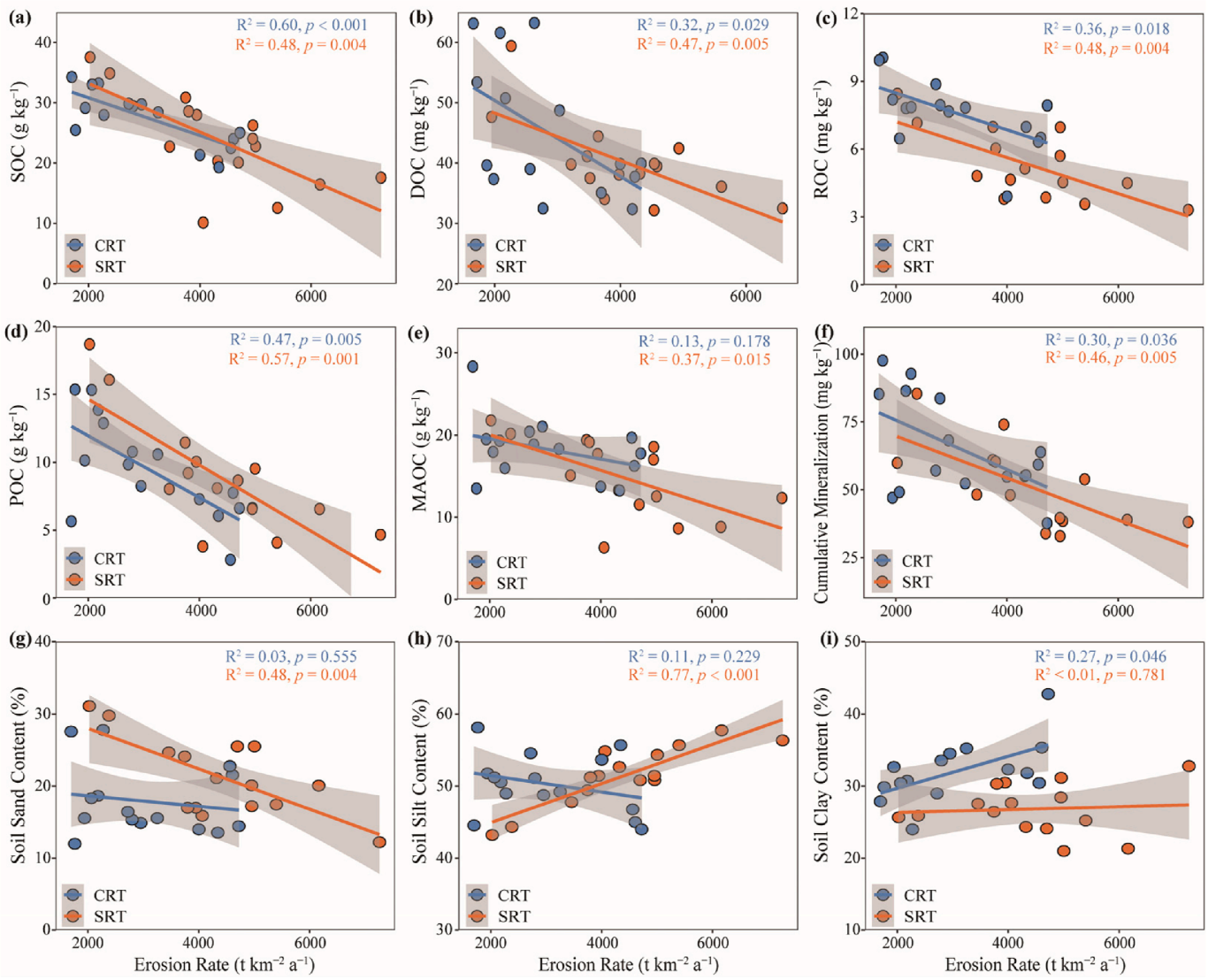

Fig. 7. The relationship between soil erosion and C fractions. SOC: Soil organic carbon; DOC: Dissolved organic carbon; ROC: Recalcitrant organic carbon; POC: particulate organic carbon; MAOC: Mineral-associated organic carbon.

Under CRT, clay content was significantly positively correlated with the amount of erosion ($p < 0.05$, Fig. 7(i)), whereas sand and silt content showed no significant correlation with the erosion rate ($p > 0.05$, Fig. 7(g) and (h)).

3.4.2. Relationship between SOC and C fractions

Further correlation analysis confirmed that soil erosion under both tillage practices significantly influenced the distribution of various C fractions. The erosion rate associated with SRT was significantly negatively correlated with SOC, DOC, ROC, POC, MAOC, and the SOC cumulative mineralization ($p < 0.05$). A strong relationship was also observed between C fractions and changes in SOC mineralization in sloping farmland. The SOC cumulative mineralization was significantly positively correlated with SOC, DOC, POC, and MAOC ($p < 0.05$), indicating that these C fractions are crucial in driving the mineralization process. Additionally, SOC was significantly positively correlated with DOC, ROC, POC, and MAOC ($p < 0.05$), suggesting that SOC dynamics are closely linked with other C forms. DOC also showed a significant positive correlation with both POC and MAOC ($p < 0.05$), while ROC was significantly positively correlated with POC ($p < 0.05$). Finally, a significant positive correlation was found between POC and MAOC ($p < 0.05$), highlighting the interconnected nature of these C fractions in sloping farmland.

The soil erosion rate in CRT exhibited a significant negative correlation with SOC, DOC, ROC, POC, and the SOC cumulative mineralization ($p < 0.05$). Additionally, a strong relationship was found between C fractions and variations in SOC mineralization in sloping farmland. The SOC cumulative mineralization was significantly positively correlated with DOC ($p < 0.05$), indicating that DOC plays a key role in driving SOC mineralization. A significant positive correlation was also observed between SOC and MAOC ($p < 0.05$), suggesting that SOC stability is linked to MAOC content. Furthermore, a significant positive relationship was identified between DOC and ROC ($p < 0.05$), highlighting the interconnectedness of these carbon forms in influencing soil carbon dynamics.

Under SRT, sand particles had a highly significant positive correlation with almost all SOC fractions ($p < 0.05$, Fig. 8(a)). In contrast, silt particles had a significant negative correlation with SOC, all carbon fractions, and SOC mineralization ($p < 0.05$, Fig. 8

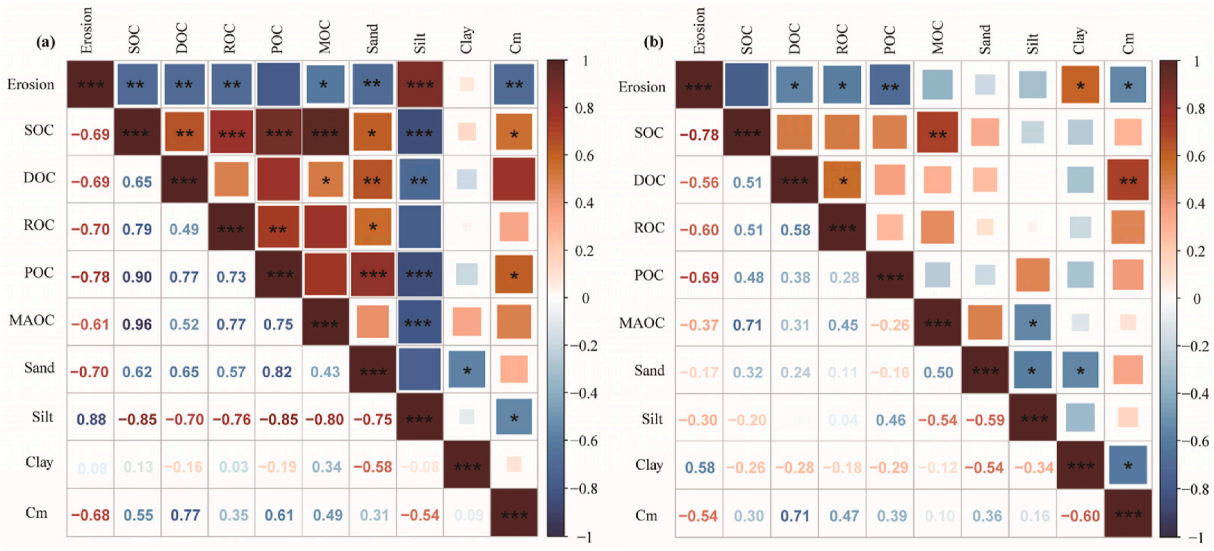

Fig. 8. The correlation between C fractions under SRT (a) and CRT (b). Erosion: Soil erosion rate; SOC: Soil organic carbon; DOC: Dissolved organic carbon; ROC: Recalcitrant organic carbon; POC: particulate organic carbon; MAOC: Mineral-associated organic carbon; *Cm*: cumulative mineralization.

(a)). However, there was no significant correlation between clay and carbon fractions ($p > 0.05$, Fig. 8(a)).Under CRT, no significant correlation between soil texture and carbon fractions was observed, and clay showed a significant negative correlation with SOC mineralization ($p < 0.05$, Fig. 8(b)).

3.4.3. *Factors affecting SOC mineralization*

A random forest importance ranking analysis was performed to evaluate the influence of various factors on SOC cumulative mineralization. The independent variables included soil erosion rate, SOC, DOC, ROC, POC, MAOC and SOC cumulative mineralization as the dependent variable. The results (Fig. 9) indicated that under SRT, the average annual soil erosion rate, SOC, and DOC content were the most significant factors affecting SOC mineralization (Fig. 9(a)). In contrast, under CRT, DOC had the greatest influence on SOC mineralization (Fig. 9(b)). This suggests that while multiple factors contribute to carbon dynamics in eroded soils, DOC plays a particularly critical role in determining SOC mineralization rates, especially in CRT.

4. Discussion

4.1. *Spatial distribution of soil erosion on slopes*

Erosion and deposition alternate along the slope, creating a distinct distribution of strong and weak erosion zones (Figs. 4 and 5). Our study revealed that the soil erosion rate exhibits periodic changes as slope length increases (Fig. 5). These findings align with the Sensoy and Kara (2014) analysis, which identified erosion peaks at 10–20 m and reduced erosion at 30–40 m on gentle slopes using ^{137}Cs. Similarly, Han et al. (2019) reconstructed gentle slopes of varying lengths and observed distinct erosion characteristics, noting a critical erosion length for slopes. The periodic variation in erosion and deposition is primarily driven by rainfall runoff. During rainfall, water flows from the top to the bottom of the slope, intensifying flow rates and erosion forces. However, once the sediment load approaches the transport capacity of the runoff, the erosion force diminishes, resulting in sediment deposition. After this unloading, flow rates and erosion forces increase again, initiating a new cycle of erosion, transport, and deposition. This

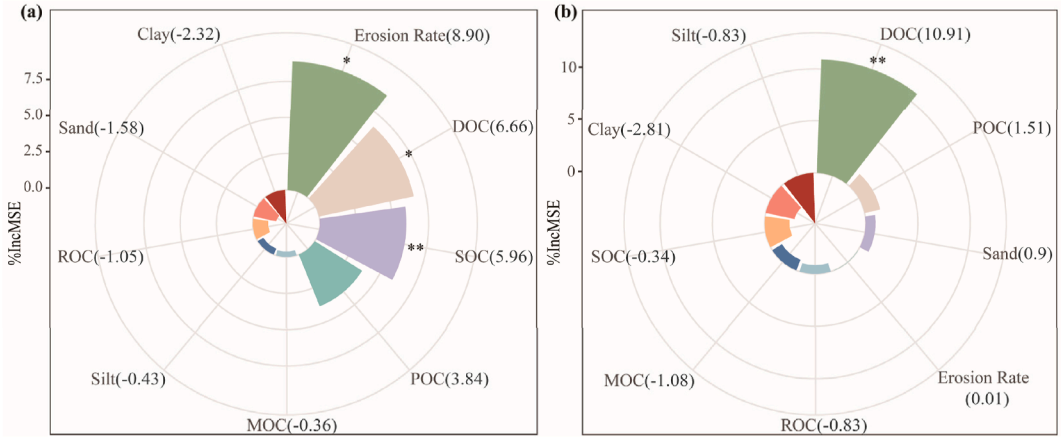

Fig. 9. Random forest analysis reveals the impact of soil erosion and C fractions on SOC mineralization under SRT (a) and CRT (b). Erosion rate: Soil erosion rate; SOC: Soil organic carbon; DOC: Dissolved organic carbon; ROC: Recalcitrant organic carbon; POC: particulate organic carbon; MAOC: Mineral-associated organic carbon.

cyclical process is evident across the slope and is highly sensitive to different tillage practices (An et al., 2014; Zhao et al., 2021, 2024). In the black soil region of Northeast China, the ^{137}Cs radionuclide tracer method was used to calculate erosion rates for typical long gentle slope farmland, allowing for comparisons of slope length sequences under different tillage practices. In this study, erosion intensity was especially affected by micro-geomorphic features, owing to the relatively high sampling density. This aligns with evidence from slopes with different micro-relief patterns: tillage-induced surface microreliefs alter the soil surface response rate to rainfall erosion by regulating runoff velocity, thereby reducing flow detachment and transport capacity. Scholand and Schmalz (2024) demonstrated through an empirical Universal Soil Loss Equation (USLE) model that contour tillage reduces soil loss on croplands in the low mountain range Gersprenz catchment in southeastern Hesse, Germany. Zhao et al. (2021) observed in farmland on the Loess Plateau of China that tillage-induced soil microrelief (TSM) is a key measure to control soil erosion. Furthermore, Fang (2021) reported that the soil, SOC and TN control efficiencies of contour tillage and hedgerow planting on the 3° and 5° plots were around 90 %, supporting CRT's efficacy across diverse pedoenvironments. The disparity in the erosion-deposition cycle between SRT and CRT is largely attributed to the runoff interception effect of the CRT. The tillage practice reduces slope flow velocity and sediment transport capacity, promoting sediment deposition within a shorter slope length cycle and initiating a new erosion cycle more quickly. Conversely, in SRT, runoff flows in the same direction as the slope, accumulating rapidly in ridge ditches and increasing water flow velocity. This concentrated flow enhances erosion forces, requiring a longer slope length cycle to reach saturation, thereby extending the erosion-deposition cycle.

4.2. Distribution patterns of SOC fractions on slopes under different tillage practices

Soil erosion is driven by raindrop impact and runoff transport, creating a complex process of soil detachment, transport, and deposition. During sediment transport and deposition, SOC undergoes internal structural changes, altering the soil structure (Abbott & Jones, 2015). Consequently, different C fractions exhibit varied responses to changes in soil environments (von Lützow et al., 2008). This study, utilizing ^{137}Cs shows that soil erosion and C fractions exhibit similar periodic fluctuations under both tillage practices along the slope (Fig. 6). SOC content was significantly negatively correlated with the average annual soil erosion rate ($p < 0.01$), and all SOC fractions (except MAOC in CRT) had significant linear relationships (Fig. 7, $p < 0.05$) with the average annual soil erosion rate, with values decreasing as erosion rates increased. These results align with prior research (Fissore et al., 2017; Hien et al., 2013; Nosrati et al., 2015; Zhang et al., 2015). As soil erosion progresses, surface SOC and C fractions are transported downslope and redeposited in lower or gentler areas. This results in a spatial redistribution of SOC and C fractions, showing periodic changes that mirror the pattern of soil erosion. Areas experiencing intense erosion show significant reductions in SOC and C fractions, while depositional areas show relative enrichment (He et al., 2023). This cyclic fluctuation of erosion and deposition directly influences the distribution pattern of SOC and C fractions, leading to synchronized fluctuations of both.

In this study, as the slope erosion rate increased, SOC and C fractions (e.g., MAOC, POC, ROC) exhibited a clear attenuation trend (Fig. 7). The more easily decomposable SOC fractions were removed first, reducing SOC content, particularly concentrated in surface soil layers (Lal, 2003; Wang et al., 2013). Soil erosion depletes SOC and exposes subsoil layers, which typically have lower SOC content. As erosion progressed, the low-carbon subsoil replaced the eroded topsoil, further reducing overall SOC and C fractions. CRT plays a pivotal role in mitigating erosion by altering the microtopography. The ridge platforms reduce water flow velocity and erosive power, promoting SOC and C fractions deposition within the ridges and furrows, thus enhancing SOC retention (Fig. 8(b)). The micro-topographic structure created by CRT effectively traps sediment and SOC, reducing the loss of SOC, especially MAOC. Since MAOC is closely bound to soil minerals and highly stable, it is better preserved under CRT, which limits its migration and promotes accumulation on the slope surface. This finding aligns with (Lv et al., 2023) who found that MAOC is better controlled under reduced erosion rates in black soil landscapes. Additionally, sediment deposition zones formed by ridge cultivation enhance MAOC enrichment, improving the stability and content of SOC.

4.3. Distribution characteristics of SOC mineralization on slopes under different tillage practices

The mineralization of SOC is a critical process in sloping farmland, with SOC being particularly vulnerable to losses induced by soil erosion. Notably, under both tillage practices, soil erosion and SOC cumulative mineralization exhibit similar fluctuation patterns along the slope (Fig. 7). Furthermore, SOC cumulative mineralization shows a significant negative correlation with the soil erosion rate (Fig. 7(f), $p < 0.05$). Soil erosion alters the soil structure, moisture conditions, and aeration by removing topsoil and exposing subsoil layers, directly influencing the SOC mineralization rate. Given the sensitivity of SOC mineralization to the soil's physical and chemical environment, fluctuations in erosion intensity led to corresponding periodic changes in mineralization rates. Soil erosion not only depletes the SOC and C fraction but also disrupts soil aggregate structure and microbial activity, accelerating the decomposition and mineralization of SOC. In areas of intense erosion, SOC losses are pronounced, accompanied by accelerated mineralization rates. Conversely, deposition zones exhibit SOC accumulation and reduced mineralization rates, resulting in periodic fluctuation patterns. The alternation between erosion and deposition processes along the slope drives the spatial periodicity in SOC distribution and its dynamic mineralization characteristics. Moreover, distinct carbon fractions, such as SOC, DOC, and POC, exhibit differential responses to erosion (Fig. 7).

The influence of tillage practices on soil carbon dynamics is markedly divergent. Under SRT, SOC loss was predominantly driven by erosion, with significant impacts observed on reactive organic carbon fractions such as DOC and POC (Fig. 9(a)). The pronounced reduction in MAOC and sand fractions was attributed to the ridges and furrows aligning with the water flow, leading to concentrated and rapid runoff that intensified surface soil erosion. Given the concentration of SOC in the topsoil, this intensified SOC mineralization. DOC is often lost in slope runoff due to the high proportion of hydrophilic compounds it contains (Maïga-Yaleu et al., 2013), while DOC and POC, as active forms of organic carbon, are particularly susceptible to erosion-induced losses. POC, which is a temporary reservoir of organic carbon bound to sand particles (53–2000 μm) in the soil (Lavallee et al., 2020) and is a less humified but more active fraction, represents a sensitive indicator of SOC dynamics (Dong et al., 2022; Fultz et al., 2013). Furthermore, sediment transport and deposition exacerbate POC mineralization through the disruption of soil aggregates (Doetterl et al., 2012; Polyakov & Lal, 2008), while reaggregation and burial in depositional zones may safeguard POC and reduce its mineralization rates (Berhe et al., 2007).

In contrast under the CRT practice, the SOC mineralization exhibited significant positive correlations only with DOC and clay content (Fig. 8(b), $p < 0.01$). CRT, characterized by ridge alignment along contour lines, effectively intercepts and decelerates water flow, mitigating large-scale SOC losses and curbing the migration and depletion of MAOC along the slope. However, DOC, due to its solubility, remained the dominant form of carbon loss in this system (Fig. 9(b), $p < 0.01$). SOC stability is closely linked to its association with soil clay particles and the structural integrity of soil aggregates. Erosion-induced disruption of aggregates facilitates the release and transport of SOC via runoff (Meliho et al., 2019; Xiao et al., 2018; Zhou et al., 2020). CRT reduces the erosive impact on SOC, potentially preserving a greater proportion of SOC for mineralization processes. Nonetheless, spatial variability in carbon mineralization was minimal, resulting in relatively uniform mineralization rates across the landscape.

In conclusion, different tillage practices significantly influence the mineralization process of SOC by altering the soil microenvironment, C source distribution, and microbial activity. SRT accelerates SOC loss and increases spatial heterogeneity, while CRT mitigates carbon loss by preserving C sources and stabilizing the soil's microenvironment.

4.4. Limitations and future perspectives

Plot-scale observations observations ($\leq$1 ha) may not fully capture watershed-level erosion dynamics, primarily reflecting localized patterns. While wavelet analysis was employed to infer spatial variations, further validation at the field scale remains necessary (Scholand & Schmalz, 2024). Although the results demonstrate significant seasonal trends, long-term monitoring is recommended to quantify cyclical variations, particularly through coupling runoff data with time-scale wavelet analysis to identify peak discharge events (Luo et al., 2021; Tong et al., 2025).

We have collaborated with the Hongxing Farm of Heilongjiang Agricultural Reclamation Group to conduct case studies from this research and demonstrated CRT's benefits, including reduced SOC loss and enhanced long-term soil fertility. Integrating CRT adoption with existing national frameworks such as the Black Soil Protection Act program of China, will amplify its impact. By mandating CRT as a best practice for sloping farmlands within these initiatives, policymakers can align local efforts with broader goals of sustainable land management and soil conservation. This comprehensive strategy, combining subsidies, education, monitoring, and policy alignment, will facilitate widespread CRT adoption and maximize its environmental and agricultural benefits.

The implementation of CRT as a sustainable agricultural practice requires coordinated policy interventions at multiple levels. Governments should establish comprehensive subsidy programs to support farmers in adopting CRT, including financial assistance for specialized equipment like contour plows and technical training on proper ridge alignment. These efforts should be particularly targeted at erosion-prone areas, where land-use regulations could mandate CRT adoption through agricultural extension services. Complementary education initiatives should leverage case studies demonstrating CRT's effectiveness in reducing SOC loss and enhancing long-term soil fertility.

This research provides compelling evidence for CRT's superiority in erosion control and SOC preservation, offering a scientifically validated approach that can be adapted globally. Successful implementation will depend on tailoring the technique to local conditions while maintaining its core principles of microtopography-driven soil conservation. The potential applications of CRT extend globally, with adaptations for different agroecological conditions, CRT could be enhanced with precision agriculture technologies. Pilot programs with real-time monitoring can demonstrate CRT's benefits and build stakeholder confidence.

5. Conclusion

This study utilized ^{137}Cs as a tracer to explore the spatial distribution of SOC and its fractions across sloped landscapes in the black soil region of Northeast China, providing a scientific foundation for assessing how soil erosion influences carbon dynamics. By quantifying the impacts of soil erosion and sediment migration on the distribution patterns of SOC and its fractions, the study revealed critical insights into the interplay between soil erosion processes and carbon sequestration. The findings demonstrate that both soil erosion rates and carbon fractions exhibit periodic fluctuations along slope length, highlighting the intricate relationship between erosion and SOC spatial distribution organization. Under SRT, SOC and its fractions generally declined with increasing erosion intensity, with SOC and DOC identified as the primary forms of carbon lost. CRT significantly mitigated erosion by modifying microtopography, particularly reducing the migration and loss of mineral-associated organic carbon (MAOC) along the slope, effectively intercepting runoff and enhancing the retention of SOC and its fractions. The study provides critical insights into the erosion-deposition dynamics of SOC and its fractions, offering a scientific foundation for optimizing erosion control strategies in long gently sloping farmland. These findings have important implications for advancing the understanding of how land management practices modulate soil carbon cycling, providing critical guidance for soil protection and sustainable agricultural practices in the black soil region of Northeast China, where soil erosion remains a pressing environmental challenge.

CRediT authorship contribution statement

Mengni Li: Writing – original draft, Visualization, Methodology, Data curation, Conceptualization. **Qingwen Zhang:** Writing – review & editing, Resources, Funding acquisition, Conceptualization. **Jeroen Meersmans:** Writing – review & editing, Supervision. **Aurore Degré:** Writing – review & editing, Supervision.

Declaration of competing interest

The authors declare that they have no known competing financial interests or per-sonal relationships that could have appeared to influence the work reported in this paper.

Acknowledgements

This work was supported by the Innovation Program of Chinese Academy of Agricultural Sciences (CAAS-CSAL-202302, CAAS-CSGLCA-IEDA-202402), and the National Natural Science Foundation of China (No. 41977072).

References

Abbott, B. W., & Jones, J. B. (2015). Permafrost collapse alters soil carbon stocks, respiration, CH_4, and N_2O in upland tundra. *Global Change Biology, 21*(12), 4570–4587. https://doi.org/10.1111/gcb.13069

Aliakbardoust, E., Adabi, M. H., Kadkhodaie, A., Harris, N. B., & Chehrazi, A. (2024). Integration of well logs and seismic attributes for prediction of thermal maturity and TOC content in the kazhdumi formation (central Persian gulf basin). *Journal of Applied Geophysics, 222*, Article 105319.

An, J., Zheng, F., & Wang, B. (2014). Using ^{137}Cs technique to investigate the spatial distribution of erosion and deposition regimes for a small catchment in the black soil region, Northeast China. *Catena, 123*, 243–251. https://doi.org/10.1016/j.catena.2014.08.009

Berhe, A. A., Harte, J., Harden, J. W., & Torn, M. S. (2007). The significance of the erosion-induced terrestrial carbon sink. *BioScience, 57*(4), 337–346. https://doi.org/10.1641/B570408

Blair, G. J., Lefroy, R. D. B., & Lisle, L. (1995). Soil carbon fractions based on their degree of oxidation, and the development of a carbon management index for agricultural systems. *Australian Journal of Agricultural Research, 46*(7), 1459–1466. https://doi.org/10.1071/AR9951459

Boros, T. (1999). Wavelet transforms: Introduction to theory and application. *Journal of Electronic Imaging, 8*(4), 478. https://doi.org/10.1117/1.482718

Borrelli, P., Robinson, D. A., Fleischer, L. R., Lugato, E., Ballabio, C., Alewell, C., … Panagos, P. (2017). An assessment of the global impact of 21st century land use change on soil erosion. *Nature Communications, 8*(1), 2013. https://doi.org/10.1038/s41467-017-02142-7

Cambardella, C. A., & Elliott, E. T. (1992). Particulate soil organic-matter changes across a grassland cultivation sequence. *Soil Science Society of America Journal, 56*(3), 777–783. https://doi.org/10.2136/sssaj1992.03615995005600030017x

Cui, M., Cai, Q., Zhu, A., & Fan, H. (2007). Soil erosion along a long slope in the gentle hilly areas of black soil region in Northeast China. *Journal of Geographical Sciences, 17*, 375–383. https://doi.org/10.1007/s11442-007-0375-4

Doetterl, S., Six, J., Van Wesemael, B., & Van Oost, K. (2012). Carbon cycling in eroding landscapes: geomorphic controls on soil organic C pool composition and C stabilization. *Global Change Biology, 18*(7), 2218–2232. https://doi.org/10.1111/j.1365-2486.2012.02680.x

Dong, L., Li, J., Liu, Y., Hai, X., Li, M., Wu, J., … Deng, L. (2022). Forestation delivers significantly more effective results in soil C and N sequestrations than natural succession on badly degraded areas: Evidence from the central loess Plateau case. *Catena, 208*, Article 105734. https://doi.org/10.1016/j.catena.2021.105734

Dungait, J. A. J., Ghee, C., Rowan, J. S., McKenzie, B. M., Hawes, C., Dixon, E. R., … Hopkins, D. W. (2013). Microbial responses to the erosional redistribution of soil organic carbon in arable fields. *Soil Biology and Biochemistry, 60*, 195–201. https://doi.org/10.1016/j.soilbio.2013.01.027

Fang, H. (2021). Impacts of rainfall and soil conservation measures on soil, SOC, and TN losses on slopes in the Black soil region, northeastern China. *Ecological Indicators, 129*, Article 108016. https://doi.org/10.1016/j.ecolind.2021.108016

Fissore, C., Dalzell, B. J., Berhe, A. A., Voegtle, M., Evans, M., & Wu, A. (2017). Influence of topography on soil organic carbon dynamics in a southern California grassland. *Catena, 149*, 140–149. https://doi.org/10.1016/j.catena.2016.09.016

Fultz, L. M., Moore-Kucera, J., Zobeck, T. M., Acosta-Martínez, V., & Allen, V. G. (2013). Aggregate carbon pools after 13 years of integrated crop-livestock management in semiarid soils. *Soil Science Society of America Journal, 77*(5), 1659–1666. https://doi.org/10.2136/sssaj2012.0423

Ganasri, B. P., & Ramesh, H. (2016). Assessment of soil erosion by RUSLE model using remote sensing and GIS - A case study of nethravathi basin. *Geoscience Frontiers, 7*(6), 953–961. https://doi.org/10.1016/j.gsf.2015.10.007

Guo, S., Zhai, L., Liu, J., Liu, H., Chen, A., Wang, H., … Lei, Q. (2019). Cross-ridge tillage decreases nitrogen and phosphorus losses from sloping farmlands in southern hilly regions of China. *Soil and Tillage Research, 191*, 48–56. https://doi.org/10.1016/j.still.2019.03.015

Han, Z., Zhong, S., Ni, J., Shi, Z., & Wei, C. (2019). Estimation of soil erosion to define the slope length of newly reconstructed gentle-slope lands in hilly mountainous regions. *Scientific Reports, 9*(1), 4676. https://doi.org/10.1038/s41598-019-41405-9

He, P., Li, P., & Sun, H. (2011). Feature extraction of acoustic signals based on complex morlet wavelet. *Procedia Engineering, 15*, 464–468. https://doi.org/10.1016/j.proeng.2011.08.088

He, Y., Zhang, F., Yang, M., Li, X., & Wang, Z. (2023). Insights from size fractions to interpret the erosion-driven variations in soil organic carbon on black soil sloping farmland, Northeast China. *Agriculture, Ecosystems & Environment, 343*, Article 108283. https://doi.org/10.1016/j.agee.2022.108283

Hien, P. D., Dung, B. D., & Phien, T. (2013). Redistributions of ^{137}Cs and soil components on cultivated hill slopes with hedgerows as conservation measures. *Soil and Tillage Research, 128*, 149–154. https://doi.org/10.1016/j.still.2012.12.003

Jones, D. L., & Willett, V. B. (2006). Experimental evaluation of methods to quantify dissolved organic nitrogen (DON) and dissolved organic carbon (DOC) in soil. *Soil Biology and Biochemistry, 38*(5), 991–999. https://doi.org/10.1016/j.soilbio.2005.08.012

Koomson, E., Muoni, T., Marohn, C., Nziguheba, G., Öborn, I., & Cadisch, G. (2020). Critical slope length for soil loss mitigation in maize-bean cropping systems in SW Kenya. *Geoderma Regional, 22*, Article e00311. https://doi.org/10.1016/j.geodrs.2020.e00311

Lal, R. (2003). Soil erosion and the global carbon budget. *Environment International, 29*(4), 437–450. https://doi.org/10.1016/S0160-4120(02)00192-7

Lal, R. (2005). Forest soils and carbon sequestration. *Forest Ecology and Management, 220*(1–3), 242–258. https://doi.org/10.1016/j.foreco.2005.08.015

Lal, R. (2019). Accelerated soil erosion as a source of atmospheric CO_2. *Soil and Tillage Research, 188*, 35–40. https://doi.org/10.1016/j.still.2018.02.001

Lal, R., Negassa, W., & Lorenz, K. (2015). Carbon sequestration in soil. *Current Opinion in Environmental Sustainability, 15*, 79–86. https://doi.org/10.1016/j.cosust.2015.09.002

Lal, R., & Pimentel, D. (2008). Soil erosion: A carbon sink or source? *Science, 319*(5866), 1040–1042. https://doi.org/10.1126/science.319.5866.1040

Lavallee, J. M., Soong, J. L., & Cotrufo, M. F. (2020). Conceptualizing soil organic matter into particulate and mineral-associated forms to address global change in the 21st century. *Global Change Biology, 26*(1), 261–273. https://doi.org/10.1111/gcb.14859

Li, M., Li, X., Shi, Y., Jiang, Y., Xue, R., & Zhang, Q. (2024). Soil enzyme activity mediated organic carbon mineralization due to soil erosion in long gentle sloping farmland in the black soil region. *The Science of the Total Environment, 929*, Article 172417.

Li, Y., Zhang, Q. W., Reicosky, D. C., Bai, L. Y., Lindstrom, M. J., & Li, L. (2006). Using ^{137}Cs and $^{210}Pb_{ex}$ for quantifying soil organic carbon redistribution affected by intensive tillage on steep slopes. *Soil and Tillage Research, 86*(2), 176–184. https://doi.org/10.1016/j.still.2005.02.006

Li, Y., Zhang, Q. W., Reicosky, D. C., Lindstrom, M. J., Bai, L. Y., & Li, L. (2007). Changes in soil organic carbon induced by tillage and water erosion on a steep cultivated hillslope in the Chinese loess Plateau from 1898-1954 and 1954-1998. *Journal of Geophysical Research, 112*, Article G01021. https://doi.org/10.1029/2005jg000107

Liu, T., Liu, X., Pan, Q., Liu, S., & Feng, X. (2023). Hydrodynamic and geochemical controls on soil carbon mineralization upon entry into aquatic systems. *Water Research, 229*, Article 119499. https://doi.org/10.1016/j.watres.2022.119499

Liu, Q. Q., Xiang, H., & Singh, V. P. (2006). A simulation model for unified interrill erosion and rill erosion on hillslopes. *Hydrological Processes, 20*(3), 469–486. https://doi.org/10.1002/hyp.5915

Luo, J., Zheng, Z., Li, T., He, S., Zhang, X., Huang, H., & Wang, Y. (2021). Quantifying the contributions of soil surface microtopography and sediment concentration to rill erosion. *Science of the Total Environment, 752*, Article 141886.

Lv, J., Shi, J., Wang, Z., Peng, Y., & Wang, X. (2023). Effects of erosion and deposition on the extent and characteristics of organic carbon associated with soil minerals in mollisol landscape. *Catena, 228*, Article 107190. https://doi.org/10.1016/j.catena.2023.107190

Maïga-Yaleu, S., Guiguemde, I., Yacouba, H., Karambiri, H., Ribolzi, O., Bary, A., … Chaplot, V. (2013). Soil crusting impact on soil organic carbon losses by water erosion. *Catena, 107*, 26–34. https://doi.org/10.1016/j.catena.2013.03.006

Mariappan, S., Hartley, I. P., Cressey, E. L., Dungait, J. A. J., & Quine, T. A. (2022). Soil burial reduces decomposition and offsets erosion-induced soil carbon losses in the Indian himalaya. *Global Change Biology, 28*(4), 1643–1658. https://doi.org/10.1111/gcb.15987

Meliho, M., Nouira, A., Benmansour, M., Boulmane, M., Khattabi, A., Mhammdi, N., & Benkdad, A. (2019). Assessment of soil erosion rates in a mediterranean cultivated and uncultivated soils using fallout 137Cs. *Journal of Environmental Radioactivity, 208–209*, Article 106021. https://doi.org/10.1016/j.jenvrad.2019.106021

Nason, G. P., & Sapatinas, T. (2002). Wavelet packet transfer function modelling of nonstationary time series. *Statistics and Computing, 12*(1), 45–56. https://doi.org/10.1023/A:1013168221710

Nelson, D. W., & Sommers, L. E. (1996). Chapter 34. Total carbon, organic carbon, and organic matter. In D. L. Sparks, A. L. Page, P. A. Helmke, R. H. Loeppert, P. N. Soltanpour, M. A. Tabatabai, C. T. Johnston, & M. E. Sumner (Eds.), *Methods of soil analysis: Part 3 chemical methods* (pp. 961–1010). Madison, WI: SSSA and ASA. https://doi.org/10.2136/sssabookser5.3.c34.

Nosrati, K., Haddadchi, A., Zare, M. R., & Shirzadi, L. (2015). An evaluation of the role of hillslope components and land use in soil erosion using ^{137}Cs inventory and soil organic carbon stock. *Geoderma, 243–244*, 29–40. https://doi.org/10.1016/j.geoderma.2014.12.008

Polyakov, V. O., & Lal, R. (2008). Soil organic matter and CO_2 emission as affected by water erosion on field runoff plots. *Geoderma, 143*(1–2), 216–222. https://doi.org/10.1016/j.geoderma.2007.11.005

Saha, A., Ghosh, P., & Mitra, B. (2018). GIS based soil erosion estimation using RUSLE model: A case study of upper kangsabati, watershed, West Bengal, India. *International Journal of Environmental Sciences & Natural Resources, 13*(5), Article 555871. https://doi.org/10.19080/IJESNR.2018.13.555871

Scholand, D., & Schmalz, B. (2024). Automated quantification of contouring as support practice for improved soil erosion estimation considering ridges. *International Soil and Water Conservation Research, 12*(4), 761–774. https://doi.org/10.1016/j.iswcr.2024.07.001

Sensoy, H., & Kara, O. (2014). Slope shape effect on runoff and soil erosion under natural rainfall conditions. *iForest: Biogeosciences and Forestry, 7*(2), 110–114. https://doi.org/10.3832/ifor0845-007

Shen, Y., Gu, J., Liu, G., Wang, X., Shi, H., Shu, C., … Zhang, Y. (2023). Predicting soil erosion and deposition on sloping farmland with different shapes in northeast China by using ^{137}Cs. *Catena, 229*, Article 107238.

Shu, X., Hu, Y., Liu, W., Xia, L., Zhang, Y., Zhou, W., & Zhang, Y. (2023). Linking between soil properties, bacterial communities, enzyme activities, and soil organic carbon mineralization under ecological restoration in an alpine degraded grassland. *Frontiers in Microbiology, 14*, Article 1131836. https://doi.org/10.3389/fmicb.2023.1131836

Tong, S., Li, G., Li, X., Li, J., Li, Y., Yue, D., … Hu, X. (2025). Influencing mechanism of microtopography on erosion hydrodynamics on bare slopes of pika mounds in alpine meadows in the yellow river source area, Western China. *Catena, 257*, Article 109158. https://doi.org/10.1016/j.catena.2025.109158

Van Hemelryck, H., Govers, G., Van Oost, K., & Merckx, R. (2011). Evaluating the impact of soil redistribution on the *in situ* mineralization of soil organic carbon. *Earth Surface Processes and Landforms, 36*(4), 427–438. https://doi.org/10.1002/esp.2055

Van Oost, K., Quine, T. A., Govers, G., De Gryze, S., Six, J., Harden, J. W., … Merckx, R. (2007). The impact of agricultural soil erosion on the global carbon cycle. *Science, 318*(5850), 626–629. https://doi.org/10.1126/science.1145724

von Lützow, M., Kögel-Knabner, I., Ludwig, B., Matzner, E., Flessa, H., Ekschmitt, K.,

… Kalbitz, K. (2008). Stabilization mechanisms of organic matter in four temperate soils: Development and application of a conceptual model. *Journal of Plant Nutrition and Soil Science, 171*(1), 111–124. https://doi.org/10.1002/jpln.200700047

Walling, D. E., He, Q., & Appleby, P. G. (2002). Conversion models for use in soil-erosion, soil-redistribution and sedimentation investigations. In F. Zapata (Ed.), *Handbook for the assessment of soil erosion and sedimentation using environmental radionuclides* (pp. 111–164). Dordrecht, Netherlands: Kluwer Academic Publishers. https://doi.org/10.1007/0-306-48054-9_7.

Wang, Z., Govers, G., Van Oost, K., Clymans, W., Van den Putte, A., & Merckx, R. (2013). Soil organic carbon mobilization by interrill erosion: Insights from size fractions. *Journal of Geophysical Research: Earth Surface, 118*(2), 348–360. https://doi.org/10.1029/2012JF002430

Wang, S., Zhao, Y., Wang, J., Gao, J., Zhu, P., Cui, X., … Lu, C. (2020). Estimation of soil organic carbon losses and counter approaches from organic materials in black soils of northeastern China. *Journal of Soils and Sediments, 20*(3), 1241–1252.

Wei, S., Zhang, X., McLaughlin, N. B., Liang, A., Jia, S., Chen, X., & Chen, X. (2014). Effect of soil temperature and soil moisture on CO_2 flux from eroded landscape positions on black soil in Northeast China. *Soil and Tillage Research, 144*, 119–125. https://doi.org/10.1016/j.still.2014.07.012

Xiao, H., Li, Z., Chang, X., Huang, B., Nie, X., Liu, C., … Jiang, J. (2018). The mineralization and sequestration of organic carbon in relation to agricultural soil erosion. *Geoderma, 329*, 73–81. https://doi.org/10.1016/j.geoderma.2018.05.018

Xu, X., Zheng, F., Wilson, G. V., He, C., Lu, J., & Bian, F. (2018). Comparison of runoff and soil loss in different tillage systems in the mollisol region of Northeast China. *Soil and Tillage Research, 177*, 1–11. https://doi.org/10.1016/j.still.2017.10.005

Zhang, X., Higgitt, D. L., & Walling, D. E. (1990). A preliminary assessment of the potential for using caesium-137 to estimate rates of soil erosion in the loess Plateau of China. *Hydrological Sciences Journal, 35*(3), 243–252. https://doi.org/10.1080/02626669009492427

Zhang, Q., & Li, Y. (2014). Effectiveness assessment of soil conservation measures in reducing soil erosion in baiquan county of Northeastern China by using ^{137}Cs techniques. *Environmental Sciences: Processes & Impacts, 16*(6), 1480–1488. https://doi.org/10.1039/C3EM00521F

Zhang, J., Quine, T. A., Ni, S., & Ge, F. (2006). Stocks and dynamics of SOC in relation to soil redistribution by water and tillage erosion. *Global Change Biology, 12*(10), 1834–1841. https://doi.org/10.1111/j.1365-2486.2006.01206.x

Zhang, J. H., Wang, Y., & Li, F. C. (2015). Soil organic carbon and nitrogen losses due to soil erosion and cropping in a sloping terrace landscape. *Soil Research, 53*(1), 87–96. https://doi.org/10.1071/SR14151

Zhang, Z., Zhang, L., Liu, Y., & Jin, M. (2024). Responses of annual streamflow variability to annual precipitation, extreme climate events and large-scale climate phenomena in the Qinghai-Tibet Plateau. *Journal of Hydrology, 632*, Article 130969.

Zhao, Q., Bai, J., Zhang, G., Jia, J., Wang, W., & Wang, X. (2018). Effects of water and salinity regulation measures on soil carbon sequestration in coastal wetlands of the yellow river Delta. *Geoderma, 319*, 219–229. https://doi.org/10.1016/j.geoderma.2017.10.058

Zhao, L., Fang, Q., Hou, R., & Wu, F. (2021). Effect of rainfall intensity and duration on soil erosion on slopes with different microrelief patterns. *Geoderma, 396*, Article 115085. https://doi.org/10.1016/j.geoderma.2021.115085

Zhao, X., Song, X., Li, L., Wang, D., Meng, P., & Li, H. (2024). Effect of microrelief features of tillage methods under different rainfall intensities on runoff and soil erosion in slopes. *International Soil and Water Conservation Research, 12*(2), 351–364. https://doi.org/10.1016/j.iswcr.2023.10.001

Zhou, S., Li, P., & Zhang, Y. (2024). Factors influencing and changes in the organic carbon pattern on slope surfaces induced by soil erosion. *Soil and Tillage Research, 238*, Article 106001. https://doi.org/10.1016/j.still.2024.106001

Zhou, M., Liu, C., Wang, J., Meng, Q., Yuan, Y., Ma, X., … Du, W. (2020). Soil aggregates stability and storage of soil organic carbon respond to cropping systems on black soils of Northeast China. *Scientific Reports, 10*(1), 265. https://doi.org/10.1038/s41598-019-57193-1

Zhu, Y., Qiu, H., Liu, Z., Ye, B., Tang, B., Li, Y., & Kamp, U. (2024). Rainfall and water level fluctuations dominated the landslide deformation at baihetan reservoir, China. *Journal of Hydrology, 642*, Article 131871.